RITG148+

THE BEST SOURCE FOR HELICAL TOMOTHERAPY® QA

RITG148+ is a precise, state-of-the-art, and comprehensive software built to perform all machine and imaging QA analyses for Helical TomoTherapy®.

Designed with the TG-148 report in mind, RITG148+ analyzes the standardized tests, including Static & Rotational Output Consistency, Jaw Centering & Alignment, Overhead Laser Positioning, Interrupted Treatment, and all others recommended for daily, monthly, and annual QA. RITG148+ also analyzes image quality using the Tomotherapy Cheese phantom.

RITG148+ software's combination of powerful, robust routines in a user-friendly interface maximize the efficiency and precision of all measurements. For added convenience, users can easily create PDF reports for all routines, as well as export their data to the RIT*trend*™ database for large-scale analysis over time.

AUTOMATED QA TESTS

- Y-jaw divergence/beam centering
- Y-jaw/gantry rotation plane alignment
- Couch translation/gantry rotation
- Gantry angle consistency
- Treatment field centering
- Interrupted treatment
- MLC alignment test
- Laser localization

IMAGE QUALITY TESTS

- Contrast
- Noise
- Uniformity
- Resolution
- CT Number to Density
- Geometric Accuracy
- Geometric Distortion
- Crop images with Pin Prick, Erase, and ROI tool

BUILT-IN FEATURES

RIT*trend*™ reporting and trending statistical database

PDF reports for every analysis routine

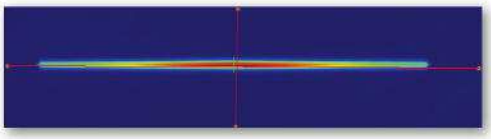

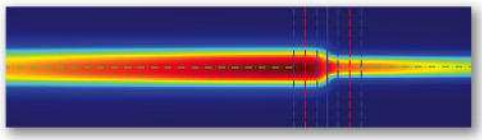

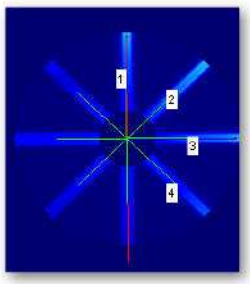

FOR MORE INFORMATION, CONTACT RIT SALES:
719.590.1077, OPT. 4 | SALES@RADIMAGE.COM

The RIT Family of Products:
Medical Physics' Leading QA Software for 25 Years

Connect with RIT
@RIT4QA

RIT™
RADIMAGE.COM

A novel computer aided breast mass detection scheme based on morphological enhancement and SLIC superpixel segmentation

Jinghui Chu, Hang Min, Li Liu, and Wei Lu[a)]
School of Electronic Information Engineering, Tianjin University, Tianjin 300072, China

(Received 23 July 2014; revised 5 April 2015; accepted for publication 11 May 2015; published 9 June 2015)

Purpose: To develop a computer-aided detection (CAD) scheme for mass detection on digitized mammograms that achieves a high sensitivity while maintaining a low false positive (FP) rate using morphological enhancement and simple linear iterative clustering (SLIC) method.
Methods: The authors developed a multiple stage method for breast mass detection. The proposed CAD scheme consists of five major components: (1) preprocessing based on morphological enhancement, which enhances mass-like patterns while removing unrelated background clutters, (2) segmentation of mass candidates based on the SLIC method, which groups mass and background tissue into different regions, (3) prescreening of suspicious regions using rule-based classification that eliminates regions unlikely to represent masses, (4) potential lesion contour refinement based on distance regularized level set evolution, and (5) FP reduction based on feature extraction and an ensemble of undersampled support vector machines. Two datasets were built to design and evaluate the system: a mass dataset containing 187 cases (386 mammograms) and a nonmass dataset containing 88 mammograms. All cases were acquired from the digital database for screening mammography (DDSM). Approximately two thirds of the available masses were used for training the system, and the remaining masses and nonmass dataset were used for testing.
Results: Testing of the proposed CAD system on the mass dataset yielded a mass-based sensitivity of 98.55%, 97.10%, 92.75% at 0.84, 0.63, 0.55 FP mark/image, respectively. Tested on the nonmass dataset, the scheme showed a FP rate of 0.55, 0.34, 0.30 mark/image.
Conclusions: The results indicate that the system is promising in improving the performance of current CAD systems by reducing FP rate while achieving relatively high sensitivity. [http://dx.doi.org/10.1118/1.4921612]

Key words: mammography, computer-aided detection, morphological enhancement, SLIC, level set, support vector machine

1. INTRODUCTION

Mammography is one of the most effective techniques for breast cancer screening and early detection. To help radiologists interpret mammograms, computer-aided detection (CAD) schemes have been developed. Recent studies have suggested that a single reading with a CAD system could be a cost-effective alternative to double reading, and that CAD systems can improve radiologists' lesion detection sensitivity.[1]

Mass lesions are high-intensity regions on mammograms and challenge CAD systems due to their ambiguous margins and irregular shapes. To solve this problem, preprocessing techniques such as enhancing and denoising methods were created to assist the mass segmentation methods. These techniques highlight the mass region or suppress the surrounding tissue. For instance, both Eltonsy[2] and Li[3] have employed morphological algorithms to assist the segmentation of mass-like regions.

Many methods have been proposed to identify mass regions. Model-based methods utilize prior knowledge for segmentation. Zheng[4] proposed a topographic feature model to define the mass lesions and eliminate false positive (FP) regions. Classifier-based methods formulate the detection problem as classifying regions as either suspicious or nonsuspicious. Clustering methods, such as *k*-means, investigate pixel features and have been proposed to group pixels together within mass regions. de Oliveira Martins[5] combined the *k*-means clustering method with the support vector machine (SVM) to identify suspicious mass regions in digital mammograms. Once mass regions are selected, contour-based methods such as level set can be conducted to refine their boundaries.[6] Examples are Yuan,[7] and Shi[8] who used level set to find the accurate border of the mass lesions.

To be viable for wide clinical use in mammography, a mass detection method should be sensitive enough that it is unlikely to miss an actual mass.[4] As to existing methods, high sensitivity usually relates to high FP detection rate. For example, to achieve 90% sensitivity, the FP rate is 1.8 marks/image from a total of 220 mammograms. While, in order to generate less than 1 FP mark/image, the sensitivity must be lower than 80%.[9] However, a high FP rate may reduce the diagnostic accuracy and the efficiency of large-scale mammography screening. Therefore, the most important technical challenge to current CAD schemes is the need for high sensitivity without producing a high FP detection rate.

In this study, we have proposed a combined detection scheme to achieve a high detection sensitivity while

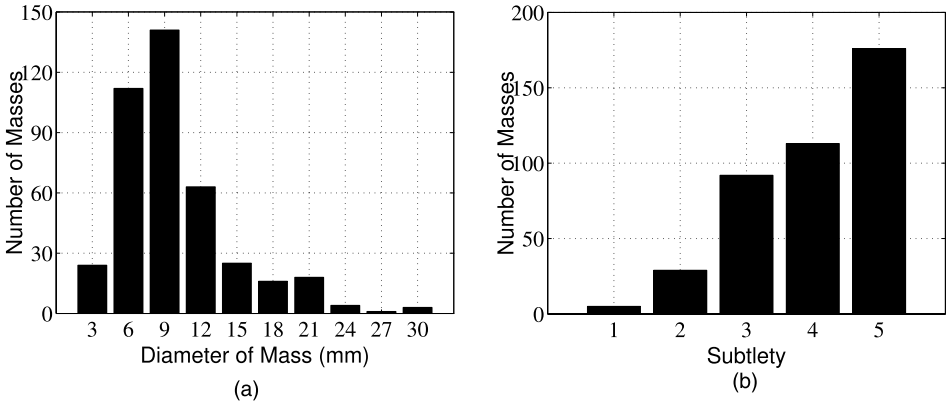

FIG. 1. (a) Diameter of masses and (b) subtlety of masses in our dataset.

maintaining a low FP rate. First, a dual morphological enhancing method was adopted to suppress interferences from blood vessels and structural noises, which can simplify the features used in the clustering method. A simple linear iterative clustering (SLIC) method was then used to isolate a set of fractions, based on intensity and spatial features. A rule-based selection was further applied to filter out nonmass candidates. After the remaining suspicious regions were refined by a level set method, an ensemble of under-sampled SVMs (EUS SVMs) scheme was applied to label a region as mass or nonmass. The approach achieved a mass-based sensitivity higher than 90% with a FP rate lower than 1 mark/image on mammograms from the DDSM.

The paper is organized as follows. Section 2 gives a brief introduction to the techniques used and discusses the experimental work in each step of the detection scheme. Section 3 presents the results, while Sec. 4 gives a discussion on the methods and results. Finally, Sec. 5 concludes the work.

2. MATERIALS AND METHODS

2.A. Dataset

The mammograms used in the study were selected from the DDSM.[10,11] The DDSM database contains four categories, i.e., normal, cancer, benign, and benign without callback. Mammograms containing suspect areas have associated ground truth information about the locations and particular types of those regions. Eighty eight normal mammograms and 187 mass cases were randomly selected from DDSM. Among them, 140 cases (286 mammograms) were from the cancer category and 47 cases (100 mammograms) were from the benign category of the DDSM database. Each mammogram in the mass cases contains at least one mass and each case contains at least one mammographic view, i.e., the craniocaudal view, the mediolateral oblique view, or both views. The mammograms used were digitized at 50 and 43.5 μm resolution, 12 bits per pixel, with a size of about 5000×3000-pixel. To speed up the processing, all images were down-sampled by a factor of 5. Therefore, the resolution of a scaled image is either 250 or 217.5 μm. Every mass region in either view is provided with a subtlety rating, indicating the difficulty level of detecting the mass. A lower subtlety rating indicates a less obvious mass and a higher difficulty level of detection.[2] Figure 1 shows the information of the masses in our dataset, including the distributions of mass size and mass subtlety. Table I shows the statistics of the dataset used in this study.

2.B. Methods

The proposed approach consists of five major stages: (1) preprocessing of mammograms, based on a dual morphological enhancing operation; (2) mass candidates segmentation, based on the SLIC method; (3) prescreening of suspicious regions, based on rule-based classification; (4) potential lesion contour refinement, based on a distance regularized level set evolution method (DRLSE); (5) FP rate reduction by using the EUS SVMs classifier. The block diagram of the detection scheme is shown in Fig. 2. These steps are described in further detail in Secs. 2.B.1–2.B.5.

Approximately two thirds of the available masses in our dataset were used for optimizing the parameters of the rule-based criteria and the EUS SVMs classifier, and the rest were used for testing. Table II contains the relevant statistics of the training and testing dataset.

2.B.1. Preprocessing based on morphological enhancement

The main difficulty of mammographic mass segmentation is that masses usually overlap with surrounding tissues. To improve the performance of mass segmentation, an image

TABLE I. Statistics of the mammogram dataset.

	Number of cases	Number of mammograms	Number of masses
Malignant	140	286	151
Benign	47	100	52
Normal	43	88	—

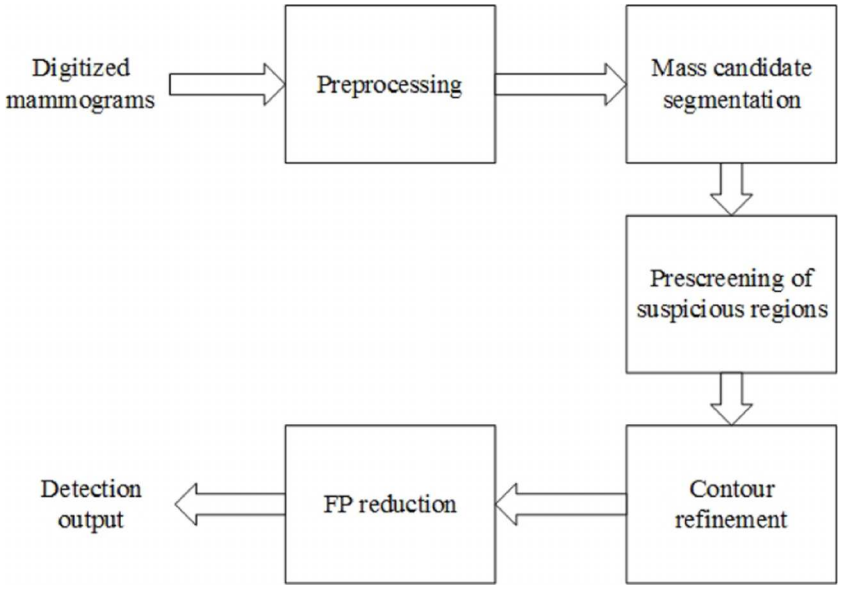

FIG. 2. Diagram of mass detection scheme.

preprocessing algorithm needs to be applied on mammograms to enhance the contrast between mass regions and background tissues.

A morphological enhancement method was applied for preprocessing. This method was originally developed by Li *et al.*[3] and then improved by Wang.[12] The algorithm is described as follows.

Step 1: Remove the objects larger than masses,

$$r_1(i,j) = \max(0,[f(i,j) - (f \circ B_1)(i,j)]), \quad (1)$$

where $f(i,j)$ is the raw mammogram, B_1 is a disk-shaped structuring element larger than the masses, and r_1 is the residue image between the original image and the opening of the original image by B_1.

Step 2: Remove the objects smaller than masses,

$$f_1(i,j) = (r_1 \circ B_2)(i,j), \quad (2)$$

where B_2 is a disk-shaped structuring element smaller than the masses. Thus, the structures whose sizes do not match masses, such as blood vessels and pectoral muscle, are removed.

Mass size varies from 3 to 30 mm in diameter,[3] which is 12–120 pixels on the mammograms resized at 250 μm resolution and approximately 14–140 pixels on the mammograms resized at 217.5 μm resolution. Thus, for images with a resolution of 250 μm, 120 and 12 pixels were chosen as the diameters of disks B_1 and B_2 in preprocessing. For images with a resolution of 217.5 μm, 140 and 14 pixels were chosen as the diameters of disks B_1 and B_2 in preprocessing.

After the preprocessing, background noises and tissues were significantly suppressed while the morphological features of the masses were well preserved. Figure 3 shows the diagram and results of the morphological enhancement.

For the convenience of future segmentation, the intensity of the enhanced image $f_1(i,j)$ was mapped to [0, 255] with a simple linear contrast stretch.

2.B.2. Mass candidate segmentation based on SLIC methods

We used a SLIC method to separate potential mass regions from the background. Based on k-means, the method separates pixels iteratively into perceptually meaningful regions, i.e., superpixels.[13] The clustering proximity is measured in spatial and intensity domain as

$$D = \sqrt{d_c^2 + \left(\frac{d_s}{S}\right)^2 m^2}, \quad (3)$$

where $d_c = \sqrt{(l_j - l_i)^2}$ describes the intensity similarity, $d_s = \sqrt{(x_j - x_i)^2 + (y_j - y_i)^2}$ describes the spatial proximity, and m is set as default value S, giving intensity and spatial proximity the same weight.

SLIC is initialized by sampling the cluster centers on a regular grid space with grid interval of S pixels. To speed up the iteration, SLIC limits the size of the search window to $2S \times 2S$ around the cluster center. The number of clusters

TABLE II. Statistics of testing and training datasets.

	Number of cases			Number of mammograms			Number of masses	
	Malignant	Benign	Normal	Malignant	Benign	Normal	Malignant	Benign
Testing	50	18	43	100	37	88	50	19
Training	90	29	—	186	63	—	101	33

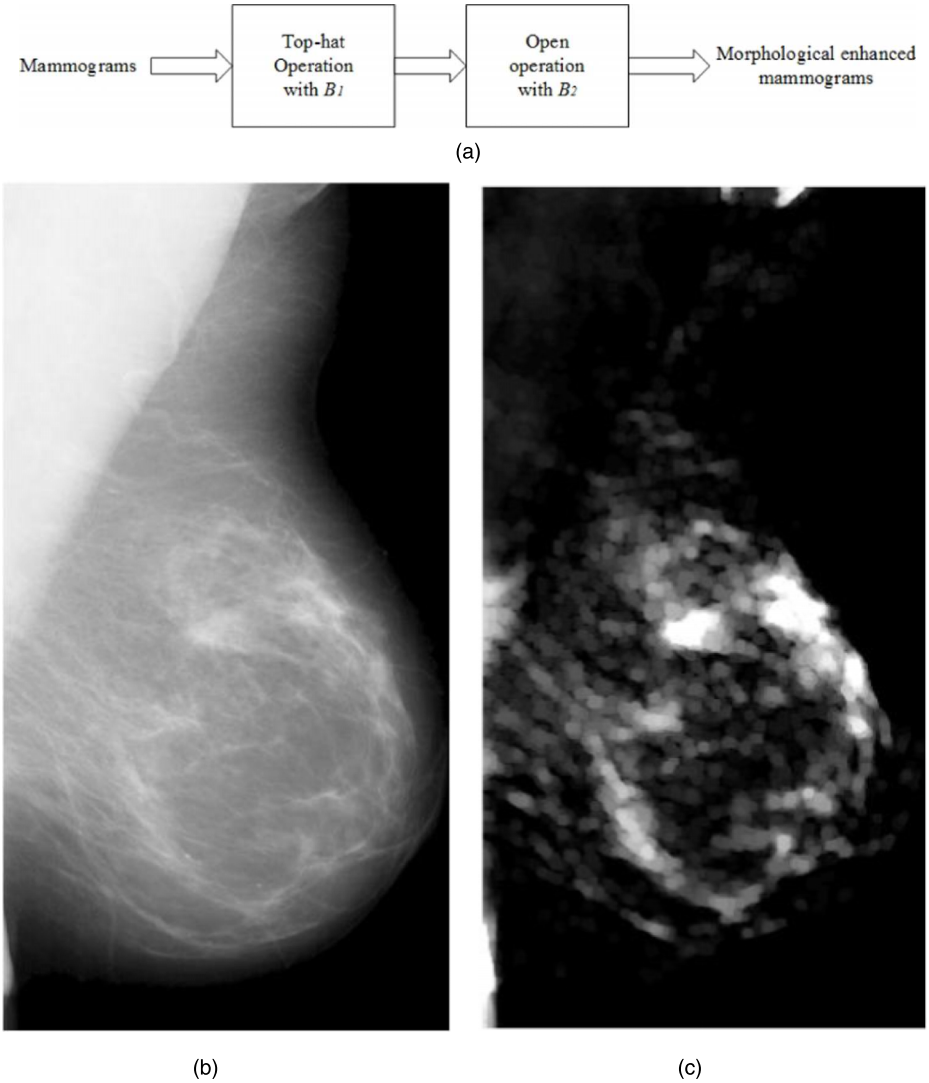

FIG. 3. (a) Diagram of morphological enhancement, (b) raw mammogram, and (c) result of dual morphological enhancement.

is adapted to the size of mammogram and breast area. The breast area is separated from the dark background by a simple thresholding method, since there is a great difference in gray level between the background (normally near 0) and the breast area. S was set as 6 pixels for images with 250 μm resolution and as 7 pixels for images with 217.5 μm resolution in this study, which corresponds to the minimum radius of mass regions. The number of clusters, k, is determined by

$$k = \left(\sqrt{\frac{N - N_B}{N_B}} + 1\right) \times \sqrt{\frac{N_B}{S^2}}, \tag{4}$$

where N_B is the number of pixels in the breast area, and N is the number of pixels in the whole mammogram.

2.B.3. Prescreening of suspicious regions based on rule-based mass classification criteria

After SLIC segmentation, each mammogram generates more than 50 superpixels in the breast area. To select suspicious regions from the SLIC results, a rule-based classification system is utilized. The training dataset was used to build the criteria. A group of statistical features, including solidity, maximum and mean gray level, topographic layer criterion,[4] and mass-background contrast are used to analyze these regions.

Masses usually have the brightest focal regions and their intensity gradually grows dimmer radially.[2] A topographic layer criterion is utilized to describe mass pattern and eliminate nonmass regions. Regions generated by the SLIC are separated into three concentric layers. Intensity variations of the three layers are analyzed to determine whether a region is a mass or not. For a mass region, the intensity of an inner layer is always higher than that of an outer layer, whereas this is not true for most nonmass regions.

Figure 4 shows how a mass region is divided into three concentric layers. L_0 stands for the region segmented by the SLIC method. R is the minimum distance from the boundary pixels to the geometrical center of the region. D is a disk-shaped structuring element. The radius of D is $0.3R$. L_1 is obtained by eroding the region with D, representing the focal area of the mass region; L_2 is obtained by subtracting L_1

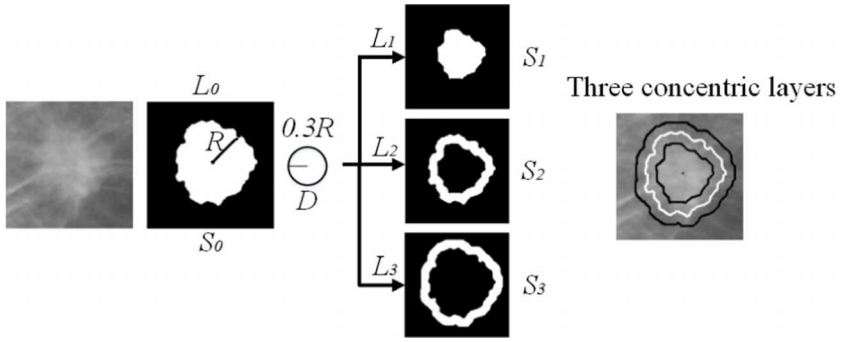

FIG. 4. Topographic layers: D is a disk structuring element with a radius of $0.3R$; $L_1 = L_0 \ominus D$, $L_2 = L_0 - L_1$, $L_3 = (L_0 \oplus D) - L_0$; S_1, S_2, and S_3 are the average value of pixels within the three layers L_1, L_2, and L_3; contrast: $(S_0 - S_3)/S_0$.

from L_0; L_3 is obtained by subtracting L_0 from the dilation of L_0 with D. L_3 represents the surrounding background area outside the mass region. S_0, S_1, S_2, S_3 are the average pixel values within the regions L_0, L_1, L_2, L_3, respectively.

The gray level reduction rate is used to describe the topographic features between two adjacent layers and mass-background contrast of the masses. The gray level reduction ratios are defined as $(S_1 - S_2)/S_1$ (first to second layer) and $(S_2 - S_3)/S_2$ (second to third layer), respectively. Mass-background contrast describes the contrast between the mass region and the surrounding area, which is defined as $(S_0 - S_3)/S_0$.

Each numerical feature mentioned above is measured on both original and enhanced mammograms for mass candidate selection, generating a pair of feature components. The corresponding classification rule is based on the distribution of the two components. Figure 5 shows the distributions of four feature pairs. After the distributions of true positive (TP) and false positive candidates are plotted, the boundary curves (as presented in the figure captions) that separate the true-positives from the false-positives are determined by trial and error and then fixed in the scheme. Each classification rule eliminates a certain number of nonmass regions. Only regions that meet every rule are selected as final mass candidates.

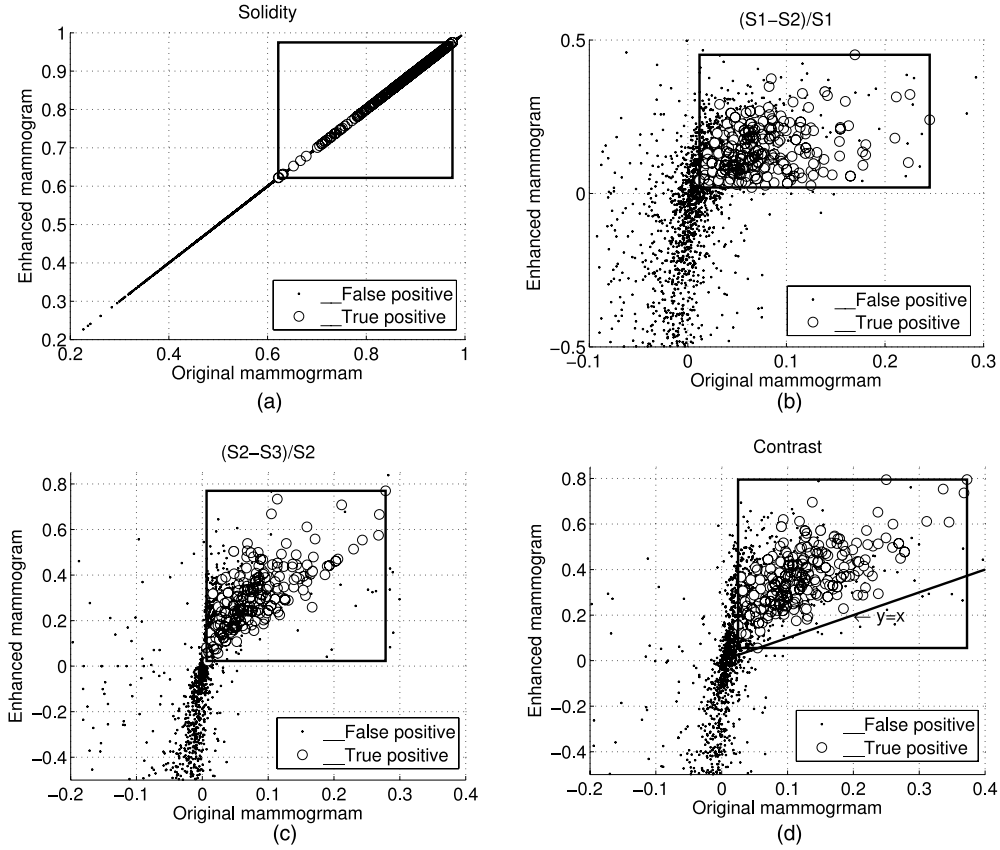

FIG. 5. Mass candidate selection criteria: (a) solidity: $\{x, y | 0.6217 \le x, y \le 0.9748\}$, (b) the gray level reduction ratio from the first layer to the second layer $(S_1 - S_2)/S_1$: $\{x, y | 0.0119 \le x \le 0.2453, 0.0194 \le y \le 0.4518\}$, (c) the gray level reduction ratio from the second layer to the third layer $(S_2 - S_3)/S_2$: $\{x, y | 0.0065 \le x \le 0.2784, 0.0229 \le y \le 0.7698\}$, and (d) contrast: $\{x, y | 0.0249 \le x \le 0.3726, 0.0555 \le y \le 0.7953, x \le y\}$.

TABLE III. Shape and size descriptor.

Shape	Size
Circularity	Area
Eccentricity	Mean radial length

TABLE IV. Texture descriptor.

Mean intensity	Standard deviation of the intensity
Entropy of the intensity distribution	Inertial momentum
Anisotropy	Entropy of the contour gradient
Topographic layer criterion	Smoothness
Skewness	Energy
Contrast	Correlation
Homogeneity	

2.B.4. Contour refinement based on DRLSE level set method

Mass segmentation in the previous step is conducted on enhanced images, which could sacrifice the subtle details of the mass contours. However, finer contours around selected regions can be retrieved from original mammograms. A level set method is used for this purpose.

Level set methods have proven useful in refining lesion contours given an initial segmentation result in many publications.[7,8] Conventional level set methods usually need to be reinitialized as a signed distance function periodically to maintain regularity. However, reinitialization can induce numerical errors and incorrectly drive the zero level set away from the expected position. This is fatal when the targets have fuzzy and irregular edges. To overcome this problem, we used the DRLSE as the refining method. DRLSE, proposed by Li *et al.*, introduced a distance regularization term to eliminate the need for reinitialization. DRLSE is able to maintain a desired shape of the level set function (LSF), particularly a signed distance profile near the zero level set. The DRLSE model is described as

$$\frac{\partial \phi}{\partial t} = \mu \mathrm{div}(d_p(|\nabla \phi|)\nabla \phi) + \lambda \delta_\varepsilon(\phi)\mathrm{div}\left(g\frac{\nabla \phi}{|\nabla \phi|}\right) + \alpha g \delta_\varepsilon(\phi), \quad (5)$$

where ϕ is the LSF. A detailed description of this evolving function of DRLSE can be found in Li *et al.*[14] The proposed DRLSE method utilizes the contours generated by SLIC as the initial LSF in our work. In the DRLSE method, when parameter α is nonzero, it gives an additional external force to drive the motion of the contour. The force causes the contour to expand when $\alpha < 0$ and shrink when $\alpha > 0$. $\alpha = -1$ is set in the first 410 iterations to expand the regions since SLIC contours only capture focal areas of masses in some cases. $\alpha = 0$ is also set for a few iterations to avoid deviation. Other parameters, i.e., λ and μ are empirically set as 5 and 0.2, respectively.

2.B.5. FP reduction based on classification

In this step, nonmass regions are further removed using the SVM.

2.B.5.a. Feature extraction. Shape and texture features are extracted from the refined suspicious regions in the original mammograms. Two shape features defined in the literature[15] and two size descriptors for classification are selected, as listed in Table III. Thirteen texture features are used to describe the smoothness and coarseness of the suspicious regions, as shown in Table IV. Details of these features can be found in the literature.[15,16]

2.B.5.b. Classification. After rule-based mass candidate selection and contour refinement, approximately one TP and four FP marks per image were identified in the training dataset. The FP instances outnumbered TP ones by nearly four times.

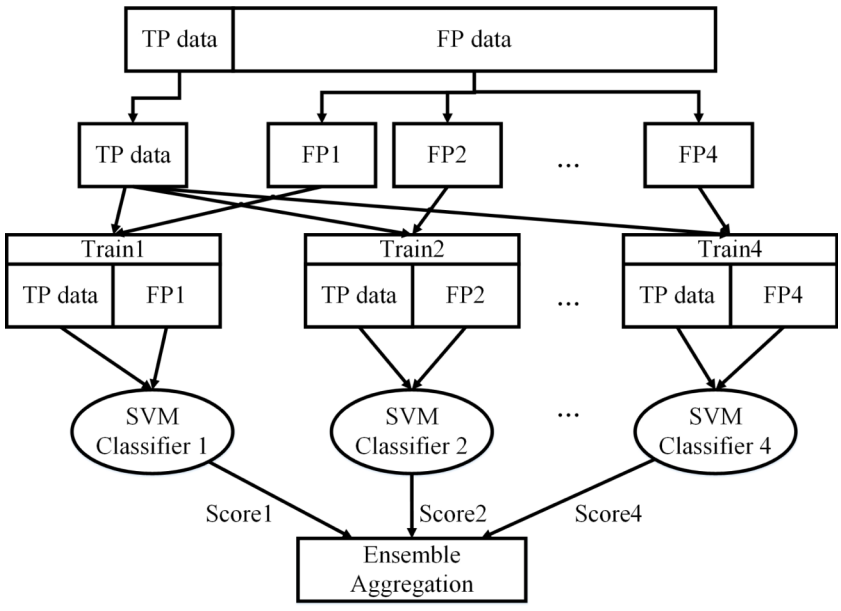

FIG. 6. EUS SVMs classification scheme.

TABLE V. Results of prescreening.

	Training dataset	Testing dataset	
		Mass dataset	Normal dataset
No. of mass regions	270	137	—
No. of detected TP ROIs	268	134	—
No. of FP ROIs	1047	518	571
No. of missing mass regions	2 benign	1 malignant, 2 benign	—
ROIs/image	5.3	4.8	6.5

According to our knowledge, the performance of SVM can be degraded when trained on an imbalanced dataset.[17] To solve this class-imbalanced problem, an EUS SVMs is applied.[18] EUS SVMs are an ensemble learning method using SVM as the basic classifier to stabilize and boost the performance of classification. The usage of EUS SVMs in this work is defined as follows.

The FP marks generated from the training mammograms set are randomly divided into four subsets FP_1, FP_2, FP_3, FP_4. Each subset is then combined with the TP dataset to form a training set $Train_i$, $i = 1, 2, 3, 4$. Each training dataset is used to construct an individual SVM classifier. Finally, the outputs of all classifiers are aggregated to decide the output according to a decision fusion rule. The diagram of EUS SVMs is shown in Fig. 6.

As for the decision fusion rule, a decision value T is used to decide the output of classification. For a testing instance, each SVM classifier generates a score $Score_i \in \{0,1\}$, "1" for mass and "0" for nonmass. Then, the sum of the scores from the four classifiers is compared with T. If $\sum Score_i \geq T$, the instance is decided as a mass, and if not, the instance is classified as a nonmass. T could be chosen from {1,2,3,4}. By tuning T, an adjustment can be made on the emphasis on the minority instances (TP instances in this case). Section 3

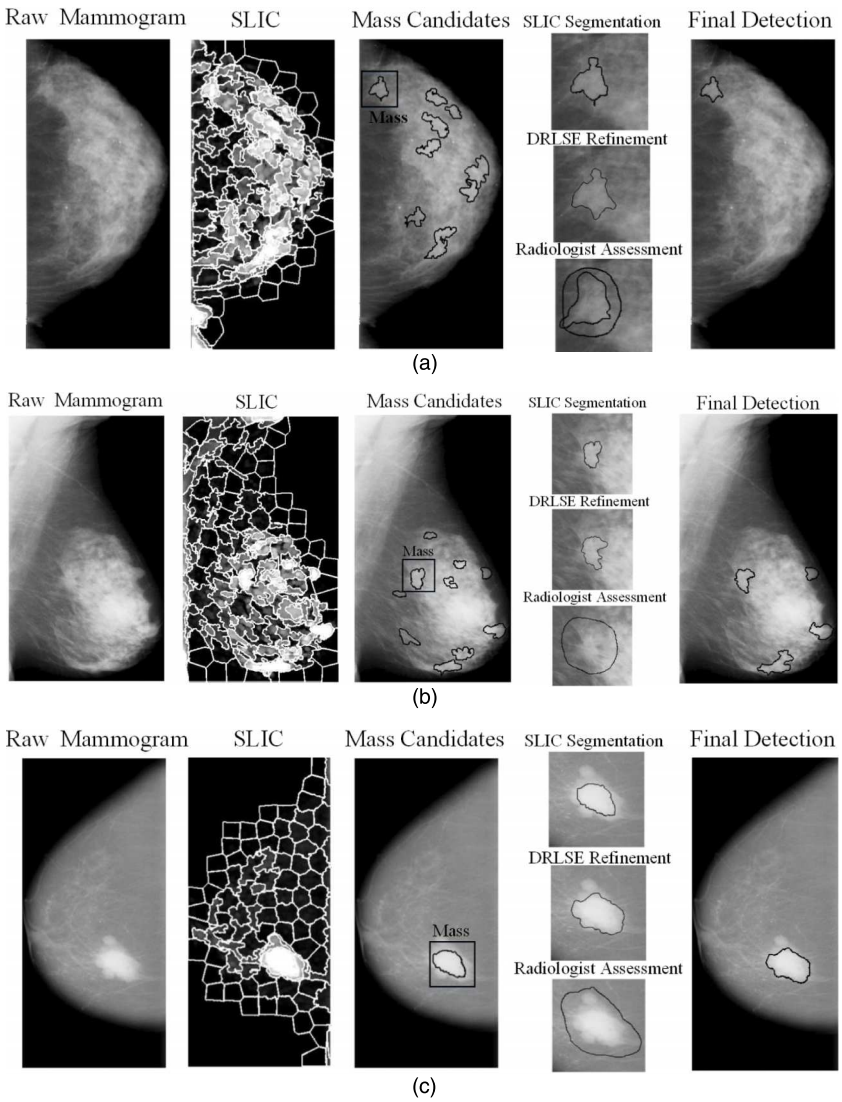

FIG. 7. (a), (b), and (c) are examples demonstrating the processing steps when $T = 1$ of our CAD scheme. From left to right are raw mammograms, SLIC segmentation on enhanced mammograms, mass ROIs selected by rule-based classification, contour comparisons between SLIC segmentation, DRLSE refinement and radiologist assessment, and final detection results after FP reduction.

TABLE VI. Region-based classification results.

Decision value	1	2	3	4
Accuracy (%)	81.37	85.19	85.80	88.24
Sensitivity (%)	93.43	90.51	86.13	84.67
Malignant sensitivity (%)	95	93	90	89
Benign sensitivity (%)	89.19	83.78	75.68	72.97
Specificity (%)	78.19	83.78	85.71	89.19
FP/image	0.84	0.63	0.55	0.42

will discuss the performance of the scheme when different T is chosen.

As for the SVM model, a library for SVM, called LIBSVM,[19] was used for training and testing. The radial basis function was used as the kernel. The cost C and kernel function parameter γ were set by a grid searching in the range of $[2^{-5},2^{5}]$ for optimal accuracy.

3. RESULTS

3.A. Suspicious mass regions identification

After the rule-based suspicious region selection, approximately 5.3 regions of interest (ROIs) on average were identified per mammogram in the training dataset. The testing and training results of prescreening are shown in Table V.

Figure 7 demonstrates the results of mass candidate segmentation and selection. It can be observed that results after DRLSE preserved more details of mass contours and adhered better to the real mass boundary.

3.B. Evaluation of classification results

EUS SVMs were trained based on the training dataset, and then the parameters were fixed for testing. The scheme was first tested on the mass testing dataset containing 68 mass cases. By varying the decision value T, a series of different testing results were achieved. Three types of results are provided, i.e., region-based, subtlety-based, and mass-based analysis. For region-based analysis, each labeled mass region was treated individually, and the sensitivity values were computed based on mass regions. The region-based results are listed in Table VI. To assess the effect of detection difficulty, the performance of the proposed scheme was also analyzed based on the subtlety rating of the mass regions. The subtlety-based results are reported in Table VII. For mass-based analysis, the same mass appearing on a two-view mammogram pair was considered to be one target, and detection of either or both regions on the two views was considered to be one TP detection. The mass-based results are listed in Table VIII. Receiver operating characteristic (ROC) curves for each SVM in EUS SVMs are shown in Fig. 8. The proposed method achieved a higher than 95% mass-based sensitivity at a FP rate lower than 1 mark/image when $T = 1$. When the region-based sensitivity is around 85%, the number of FP marks/image is less than 0.5. As shown in Table VI, the smaller the decision value T is, the more attention is paid to mass instances and the higher sensitivity and FP rates are achieved. Further, the system always achieved a FP rate of lower than 1 mark/image.

TABLE VII. Subtlety-based classification results.

Subtlety	Decision value 1	2	3	4
≤2	91.67% (11/12)	91.67% (11/12)	66.67% (8/12)	66.67% (8/12)
3	86.67% (26/30)	86.67% (26/30)	83.33% (25/30)	80.00% (24/30)
4	94.12% (32/34)	91.18% (31/34)	88.24% (30/34)	88.24% (30/34)
5	96.72% (59/61)	91.80% (56/61)	90.16% (55/61)	88.52% (54/61)

TABLE VIII. Mass-based classification results.

Decision value	1	2	3	4
Sensitivity (%)	98.55	97.10	92.75	92.75

The proposed CAD scheme was also evaluated on the normal dataset with 88 normal mammograms. The results are listed in Table IX, which shows the system can also achieve less than 1 mark/image on normal mammograms.

4. DISCUSSION

In this study, we developed a breast mass detection scheme on digitized mammograms and demonstrated its performance

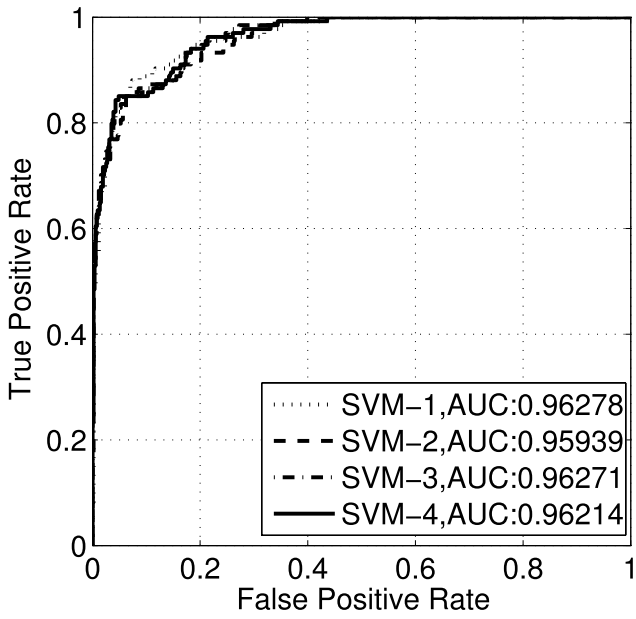

FIG. 8. EUS SVMs ROC curves.

TABLE IX. Normal cases detection results.

Decision value	1	2	3	4
FP/image	0.55	0.34	0.30	0.21
Percentage of images without FP detection (%)	55.68	70.45	73.86	79.55
Percentage of cases without FP detection (%)	34.88	46.51	53.49	65.12

TABLE X. Comparison between different classifiers.

	LM			
Performance	ANN (%)	LDA (%)	SVM (%)	EUS SVMs (T = 2) (%)
Accuracy	92.98	92.37	92.67	85.19
Sensitivity	70.07	80.29	78.83	90.51
Specificity	99.03	95.56	96.33	83.78

on a public mammography dataset. The proposed method can achieve a relatively low FP rate while maintaining satisfactory accuracy and sensitivity.

Morphological preprocessing enhances the masslike regions and suppresses the negative impacts induced by blood vessels and structural noises. This characteristic can be observed in Fig. 5(d) where the TP feature points are above the line $y = x$, which means mass-background contrast was enhanced. Morphological enhancement can effectively improve the performance of detection. As shown in Fig. 9, applying SLIC directly on original mammograms usually causes boundary leakage due to the low contrast between mass regions and surrounding tissues. However, segmentation results on enhanced images demonstrate better adherence to the mass boundary. Introducing morphological enhancement as a preprocessing procedure before the clustering segmentation can simplify the features used in the clustering algorithm and reduce the computational complexity of clustering. The method developed by de Oliveira Martins *et al.*[5] uses a k-means clustering method based on numerous texture features on raw mammograms to segment mass regions. Compared to the previous method, the proposed method can achieve a satisfactory segmentation performance based solely on gray level and spatial information due to the contribution of morphological enhancement.

In the rule-based prescreening, topographic layer criterion was described by analyzing the intensity differences between the three layers. For a mass region, the intensity grows dimmer radially. As shown in Figs. 5(b) and 5(c), the TP feature points are above $y = 0$ and on the right of $x = 0$, indicating that the average pixel value of an inner layer is greater than that of an outer layer. Preliminary results show that the combination of topographic layer criterion and other rules reduces the FP detection rate effectively while yielding a high sensitivity.

The DRLSE level set method was used to refine SLIC segmentation contour. Compared with other level set methods,

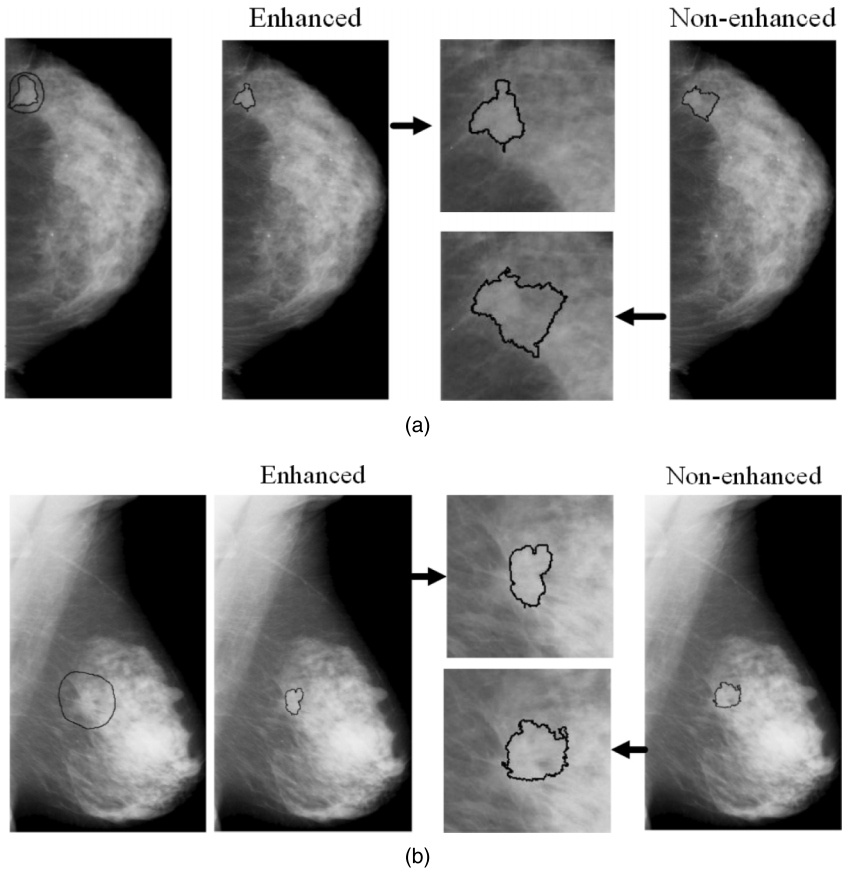

FIG. 9. SLIC segmentation results on morphological enhanced mammograms and on raw mammograms.

TABLE XI. Performance comparison between our CAD scheme and other CAD systems.

Publications	Sensitivity		FP/image
	Region-based (%)	Mass-based (%)	
Wei *et al.* (2005) (Ref. 9)	—	70, 80, 90	0.72, 1.08, 1.82
Bellotti *et al.* (2006) (Ref. 21)	80	—	4.23
Eltonsy *et al.* (2007) (Ref. 2)	—	81, 88, 92	0.6, 2.4, 5.4
de Oliveira Martins *et al.* (2009) (Ref. 20)	89.3	—	0.93
de Oliveira Martins *et al.* (2009) (Ref. 5)	86	—	1.2
Kozegar *et al.* (2013) (Ref. 22)	80, 90	—	2.5, 4.5
Our work	86.1, 90.5, 93.4	92.7, 97.1, 98.5	0.55, 0.63, 0.84

DRLSE is reinitialization-free and able to maintain regularity of LSF. It provides more accurate shape information of mass candidates for the next stage of classification and helps to improve the classification performance.

In this study, the sensitivity for malignant masses is higher than that of benign masses, as indicated in Table VI. This is mainly because the dataset contains less benign cases than malignant ones. However, this is acceptable since the detection performance of a CAD scheme for malignant masses is more important than its performance for all masses.

EUS SVMs are an ensemble learning method targeting class imbalance problem. The ensemble undersampled structure is the key to solving the imbalance problem. Table X lists performance comparisons on the imbalanced dataset between EUS SVMs and three standard learning machines (LM): artificial neural network (ANN), linear discriminant analysis (LDA), and SVM. The table shows that the mass detection rate can be degraded when applying a standard learning machine directly on an imbalanced dataset. EUS SVMs can achieve a higher sensitivity on imbalanced inputs than the other classic learning machines.

The detection performance of the system on masses with different subtlety is shown in Table VII. When $T \leq 2$, the detection rate of masses with subtlety ≤ 2 remains the same. When $T = 3$, the detection rate drops to lower than 70%. This means that not all SVM classifiers in the EUS SVMs can identify subtle masses successfully. The ensemble structure of EUS SVMs and adjustment of T compensate for the drawback of a single undersampled learning machine. The detection of subtle masses is sensitive to T. For the EUS SVMs classifier, when the TP to FP ratio is roughly 1 to N, N SVM classifiers should be used and $T \in \{1,\ldots,N\}$. Normally, when $T = N/2$, the sensitivity and specificity are well-balanced. This was observed in the experiments. When $T = 2$, the scheme achieved a relatively high sensitivity together with a relatively low FP rate.

The proposed method (with $T = 1,2,3$) is compared with existing methods in Table XI in terms of the sensitivity and FP rate. It is worth noting that the schemes proposed in the other relevant literatures[2,5,20] were also evaluated on the DDSM database. These results indicate that the proposed scheme has the potential to lower the FP rate of CAD without sacrificing sensitivity.

The major limitation of the proposed CAD scheme is that some of the key parameters were empirically selected and optimized. To make the CAD scheme robust for wide clinical use, a more sophisticated approach for parameter selection and optimization is certainly desirable. We are currently investigating the possibility of adopting more comprehensive and automated parameter optimization methods.

5. CONCLUSION

We developed an advanced scheme for mass detection on digitized mammograms and demonstrated its performance on a DDSM dataset. Mass segmentation was conducted using morphological enhancement combined with the SLIC method. Morphological enhancement is effective in suppressing the interferences of the breast tissue and structural noises surrounding the mass regions. By enhancing the contrast between masses and the surrounding tissue, morphological enhancement enables the clustering method SLIC to achieve a satisfactory segmentation performance based on simple features, such as intensity and spatial distance. To reduce the number of FP results, a rule-based classification and EUS SVMs classifier were employed. Further, between the two FP reducing steps, DRLSE level set method was used to refine the contour of potential mass candidates, providing more reliable mass region information for the SVM classification in the following stage. The proposed scheme achieved a satisfactory sensitivity while maintaining a relatively low false positive rate, which indicates that the scheme can be a good starting point for future improvement and is promising in enhancing the performance of current CAD systems.

[a]Electronic mail: luwei@tju.edu.cn

[1]J. Wei, H.-P. Chan, C. Zhou, Y. T. Wu, B. Sahiner, L. M. Hadjiiski, M. A. Roubidoux, and M. A. Helvie, "Computer-aided detection of breast masses: Four-view strategy for screening mammography," Med. Phys. **38**, 1867–1876 (2011).

[2]N. H. Eltonsy, G. D. Tourassi, and A. S. Elmaghraby, "A concentric morphology model for the detection of masses in mammography," IEEE Trans. Med. Imaging **26**, 880–889 (2007).

[3]H. Li, Y. Wang, K. J. R. Liu, S.-C. B. Lo, and M. T. Freedman, "Computerized radiographic mass detection. I. Lesion site selection by morphological enhancement and contextual segmentation," IEEE Trans. Med. Imaging **20**, 289–301 (2001).

[4]B. Zheng, Y.-H. Chang, and D. Gur, "Computerized detection of masses in digitized mammograms using single-image segmentation and a multilayer topographic feature analysis," Acad. Radiol. **2**, 959–966 (1995).

[5]L. de Oliveira Martins, G. B. Junior, A. C. Silva, A. C. de Paiva, and M. Gattass, "Detection of masses in digital mammograms using K-means and

support vector machine," Electron. Lett. Comput. Vision Image Anal. **8**(2), 39–50 (2009).
[6]A. Oliver, J. Freixenet, J. Martí, E. Pérez, J. Pont, E. R. E. Denton, and R. Zwiggelaar, "A review of automatic mass detection and segmentation in mammographic images," Med. Image Anal. **14**, 87–110 (2010).
[7]Y. Yuan, M. L. Giger, H. Li, K. Suzuki, and C. Sennett, "A dual-stage method for lesion segmentation on digital mammograms," Med. Phys. **34**, 4180–4193 (2007).
[8]J. Shi, B. Sahiner, H.-P. Chan, J. Ge, L. Hadjiiski, M. A. Helvie, A. Nees, Y.-T. Wu, J. Wei, C. Zhou, C. Y. Zhang, and J. Cui, "Characterization of mammographic masses based on level set segmentation with new image features and patient information," Med. Phys. **35**, 280–290 (2008).
[9]J. Wei, B. Sahiner, L. M. Hadjiiski, H.-P. Chan, N. Petrick, M. A. Helvie, M. A. Roubidoux, J. Ge, and C. Zhou, "Computer-aided detection of breast masses on full field digital mammograms," Med. Phys. **32**, 2827–2838 (2005).
[10]M. Heath, K. Bowyer, D. Kopans, R. Moore, and W. P. Kegelmeyer, "The digital database for screening mammography," in *Proceedings of the 5th International Workshop on Digital Mammography*, edited by M. J. Yaffe (Medical Physics Publishing, 2001), pp. 212–218.
[11]"Current status of the digital database for screening mammography," in *Digital Mammography*, edited by M. Heath, K. Bowyer, D. Kopans, W. P. Kegelmeyer, R. Moore, K. Chang, and S. MunishKumaran (Springer, Netherlands, 1998), pp. 457–460.
[12]Y. Wang, "Computer-aided detection and analysis of mammographic mass," Ph.D. thesis, Xidian University, 2010.
[13]R. Achanta, A. Shaji, K. Smith, A. lien Lucchi, P. Fua, and S. Süsstrunk, "Slic superpixels," EPFL Technical Report No. 149300, 2010.
[14]C. Li, C. Xu, C. Gui, and M. D. Fox, "Distance regularized level set evolution and its application to image segmentation," IEEE Trans. Image Process. **19**, 3243–3254 (2010).
[15]D. Cascio, F. Fauci, R. Magro, G. Raso, R. Bellotti, F. D. Carlo, S. Tangaro, G. D. Nunzio, M. Quarta, G. Forni, A. Lauria, M. E. Fantacci, A. Retico, G. L. Masala, P. Oliva, S. Bagnasco, S. C. Cheran, and E. L. Torres, "Mammogram segmentation by contour searching and mass lesions classication with neural network," IEEE Trans. Nucl. Sci. **53**, 2827–2833 (2006).
[16]N. Pradeep, H. Girisha, B. Sreepathi, and K. Karibasappa, "Feature extraction of mammograms," Int. J. Bioinf. Res. **4**, 241–244 (2012).
[17]R. Akbani, S. Kwek, and N. Japkowicz, "Applying support vector machines to imbalanced datasets," in *Machine Learning: ECML 2004* (Springer, Berlin, Heidelberg, 2004), pp. 39–50.
[18]P. Kang and S. Cho, "EUS SVMs: Ensemble of under-sampled SVMs for data imbalance problems," in *Neural Information Processing* (Springer, Berlin, Heidelberg, 2006), pp. 837–846.
[19]C.-C. Chang and C.-J. Lin, "A library for support vector machines," ACM Trans. Intell. Syst. Technol. **2**, 1–27 (2011).
[20]L. de Oliveira Martins, A. C. Silva, A. C. de Paiva, and M. Gattass, "Detection of breast masses in mammogram images using growing neural gas algorithm and Ripley's K function," J. Signal Process. Syst. **55**, 77–90 (2009).
[21]R. Bellotti, F. D. Carlo, and S. Tangaro, "A completely automated CAD system for mass detection in a large mammographic database," Med. Phys. **33**, 3066–3075 (2006).
[22]E. Kozegar, M. Soryani, B. Minaei, and I. Domingues, "Assessment of a novel mass detection algorithm in mammograms," J. Cancer Res. Ther. **9**(4), 592–600 (2013).